


Article

Structural, Surface, and Optical Properties of AlN Thin Films Grown on Different Substrates by PEALD

Sanjie Liu ¹, Yangfeng Li ² , Jiayou Tao ¹, Ruifan Tang ^{1,*} and Xinhe Zheng ^{3,*}

¹ Key Laboratory of Hunan Province on Information Photonics and Freespace Optical Communications, School of Physics and Electronic Science, Hunan Institute of Science and Technology, Yueyang 414006, China; liusanjie@hnist.edu.cn (S.L.); 12015013@hnist.edu.cn (J.T.)

² College of Semiconductors (College of Integrated Circuits), Hunan University, Changsha 410082, China; liyangfeng12@mails.ucas.ac.cn

³ Beijing Key Laboratory for Magneto-Photoelectrical Composite and Interface Science, School of Mathematics and Physics, University of Science and Technology, Beijing 100083, China

* Correspondence: 12022055@hnist.edu.cn (R.T.); xinhezhen@ustb.edu.cn (X.Z.)

Abstract: Plasma-enhanced atomic layer deposition was employed to grow aluminum nitride (AlN) thin films on Si (100), Si (111), and c-plane sapphire substrates at 250 °C. Trimethylaluminum and Ar/N₂/H₂ plasma were utilized as Al and N precursors, respectively. The properties of AlN thin films grown on various substrates were comparatively analyzed. The investigation revealed that the as-grown AlN thin films exhibit a hexagonal wurtzite structure with preferred c-axis orientation and were polycrystalline, regardless of the substrates. The sharp AlN/substrate interfaces of the as-grown AlN are indicated by the clearly resolved Kiessig fringes measured through X-ray reflectivity. The surface morphology analysis indicated that the AlN grown on sapphire displays the largest crystal grain size and surface roughness value. Additionally, AlN/Si (100) shows the highest refractive index at a wavelength of 532 nm. Compared to AlN/sapphire, AlN/Si has a lower wavelength with an extinction coefficient of zero, indicating that AlN/Si has higher transmittance in the visible range. Overall, the study offers valuable insights into the properties of AlN thin films and their potential applications in optoelectronic devices, and provides a new technical idea for realizing high-quality AlN thin films with sharp AlN/substrate interfaces and smooth surfaces.

Keywords: aluminum nitride; thin films; different substrates; plasma-enhanced atomic layer deposition



Citation: Liu, S.; Li, Y.; Tao, J.; Tang, R.; Zheng, X. Structural, Surface, and Optical Properties of AlN Thin Films Grown on Different Substrates by PEALD. *Crystals* **2023**, *13*, 910. <https://doi.org/10.3390/cryst13060910>

Academic Editor: Evgeniy N. Mokhov

Received: 13 April 2023

Revised: 27 May 2023

Accepted: 31 May 2023

Published: 3 June 2023



Copyright: © 2023 by the authors. Licensee MDPI, Basel, Switzerland. This article is an open access article distributed under the terms and conditions of the Creative Commons Attribution (CC BY) license (<https://creativecommons.org/licenses/by/4.0/>).

1. Introduction

Aluminum nitride (AlN) is a highly promising wide-bandgap semiconductor because of its excellent thermal conductivity (single crystal: 285 W/m·K), along with its superior chemical stability and electrical insulation, which makes it a highly attractive material for high-electron-mobility transistors, light-emitting diodes, and laser diodes [1–4]. AlN is often utilized as a buffer layer for gallium nitride (GaN) in semiconductor device fabrication, reducing defects by providing a smooth and compatible interface between the substrate and the GaN layer [5–9]. Molecular beam epitaxy, sputtering, and metal–organic chemical vapor deposition are conventional methods used to grow high-quality AlN epilayers [10–13]. In general, these methods require elevated temperatures to achieve high-quality films and ensure adequate throughput. Unfortunately, high process temperatures yield additional stresses on the film stacks, which are not suitable for the fabrication of AlN films for sensory applications [14]. Therefore, alternative approaches are required to control the thickness of AlN films at relatively low temperatures for these specific applications.

Atomic layer deposition (ALD) is an attractive alternative low-temperature technique for preparing AlN thin films [15–20]. The deposition process relies on chemical surface reactions triggered by sequential precursor dosing. Precursors in the vapor phase chemisorb onto the surface via self-limiting reactions, wherein only the monolayer reacts [21–23]. This

feature enables deposition on structures with high aspect ratios, facilitating the formation of thin films. Therefore, the film thickness can be accurately regulated by adjusting the number of reaction cycles. Plasma-enhanced ALD (PEALD) is a modified version of the conventional ALD technique used for depositing thin films of various materials with precise control over their thickness and composition. In PEALD, a plasma source is used to generate reactive species that can react with the precursor molecules and facilitate the deposition process. The plasma can also provide energy to the growing film, leading to lower deposition temperature, improved film quality, and enhanced step coverage [20].

In the literature, ALD and PEALD of AlN thin films have been extensively studied [24–31]. Polycrystalline AlN films were produced via both ALD and PEALD. The roughness of AlN films increased with higher deposition temperature and thicker film [31]. Tarala et al. obtained crystalline AlN using PEALD at temperatures less than 300 °C [32]. Shih et al. used ALD to deposit high-quality single-crystal hexagonal AlN, employing in-situ treatment. When these films were grown on GaN, the researchers observed increased mobility and sheet electron concentration [33]. Legallais et al. reported that adjusting ion energy through substrate biasing during the PEALD process significantly improved the quality of AlN [34]. Kim et al. deposited AlN on a GaN substrate using thermal ALD, and studied the interfacial properties of the ALD-AlN/GaN interface [35,36]. Bui et al. investigated the growth behavior and optical properties of ALD-AlN, revealing an increase in the refractive index with increasing film thickness and growth temperature [26,37]. Schiliro et al. obtained AlN with a predominant crystallographic orientation along the *c*-axis, with excellent alignment on GaN-sapphire substrates, resulting in high-density two-dimensional electron gas formation at the interface [38]. However, there have been relatively few studies conducted on how substrates impact the properties of AlN deposited via PEALD.

This study aimed to investigate and compare the characteristics of AlN films formed on different substrates, including Si (111) *c*-plane sapphire and Si (100), via PEALD at a temperature of 250 °C. The as-grown AlN films were polycrystalline, with a clear preference for the (002) orientation. Additionally, the interfaces between the films and substrates were extremely sharp. Surface morphology analysis revealed that the crystal grain size and surface roughness were highest for AlN films grown on sapphire, while the refractive index was highest for AlN/Si (100) at a wavelength of 532 nm. AlN/Si had a lower extinction coefficient than AlN/sapphire, indicating higher transmittance in the visible range.

2. Experimental

The deposition of AlN thin films was carried out using a PEALD process in an Angstrom-dep III reactor. The nitrogen and gallium precursors were trimethylaluminum (TMA) and a gas mixture containing Ar, N₂, and H₂ with a 1:3:6 ratio, respectively. The Si and sapphire substrates used in our experiments were wafers with a diameter of 2 inches. Prior to the growth experiments, we cleaned the sapphire substrates sequentially in an ultrasonic bath with isopropanol and acetone, followed by methanol and deionized water, while the Si was cleaned using the RCA standard cleaning process. The reactor was loaded with these substrates immediately, and the base pressure of the process was tuned to around 0.15 Torr. Subsequently, the substrate chuck was resistively heated to the growth temperature and given 20 min to reach thermal equilibrium. To enhance the crystalline quality and eliminate possible nucleation delays, the deposition cycles were preceded by a nitridation process step under 60 W rf-plasma power. Ar/N₂/H₂ (1:3:6) plasma was applied for 30 s, and the gas flow was set to 5 sccm. Then, deposition of AlN was carried out using the optimized PEALD-AlN parameters reported in our previous work [39], where the details are as follows: 15 s plasma/25 s N₂ purge /0.05 s TMA/25 s N₂ purge. During the experiment, the substrate temperature was maintained at 250 °C, and a total of 500 growth cycles were conducted.

X-ray photoelectron spectroscopy (XPS) was utilized to obtain information about the elemental composition, chemical state, and bonding of the AlN films. The instrument used was an ESCALAB 250Xi, which used an Al Kα X-ray source that was monochromatized.

Spectroscopic ellipsometry (SE) measurements were performed to determine the optical properties of the AlN films, covering the optical spectrum from 730 to 280 nm at an incidence angle of 70° . The spectra obtained from the measurements were analyzed to extract the thickness of the films. To assess the crystallinity of the GaN thin films, grazing incidence X-ray diffraction (GIXRD) was conducted. X-ray reflectometry (XRR) measurements were carried out to study the AlN/substrate interfacial property. Both GIXRD and XRR measurements are performed with a Smartlab system. The voltage and current were 40 kV and 30 mA, respectively. To enhance the intensity of X-rays diffracted from the thin film and avoid signals from the substrate, we conducted GIXRD measurements at a low grazing angle of 0.65° . Cross-sectional AlN was characterized using scanning electron microscopy (SEM, Zeiss supra55). The surface morphology of the samples was analyzed using the Micronano D-5A atomic force microscope (AFM) system. The scanning area was $1 \times 1 \mu\text{m}^2$.

3. Results and Discussion

GIXRD analysis was conducted to determine the crystalline nature of the AlN thin films, and the obtained patterns (see Figure 1) exhibited diffraction peaks corresponding to the (100), (002), (101), and (110) planes of the hexagonal wurtzite phase, based on PDF#25-1133, indicating no mixing of other phases such as cubic. The analysis suggests that polycrystalline hexagonal AlN (h-AlN) films were obtained, displaying a dominant (002) orientation, regardless of the substrate used. Previous studies have suggested that ALD-deposited AlN films tend to crystallize in the (100) orientation [40,41], and sputtered AlN films that are more frequently reported to have c-plane orientation [42,43]. To obtain a preferred orientation of (002), the surface atoms must undergo kinetic energy-driven rearrangement to achieve a configuration with the minimum surface energy. When considering the steric hindrance of methyl groups, the low-density (100) plane could be even more beneficial because the mobility of atoms is diminished in low-temperature. Alevli et al. reported that AlN films exhibit (100) preferred orientation when grown at a low temperature of 185°C , and the predominance of the (002) orientation becomes more prominent for AlN synthesized at elevated temperatures growth conditions. However, the AlN with a preferred orientation of (002) in the present work may be attributed to highly reactive radicals produced by Ar/N₂/H₂ plasma. The diffraction patterns of AlN samples exhibit similarities, but there is a difference in peak intensities: The (002) peak intensity in AlN/Si (111) was observed to be comparatively greater than that in AlN/Si (100) and AlN/sapphire. The location and width of the AlN (002) reflections in GIXRD are summarized in Table 1.

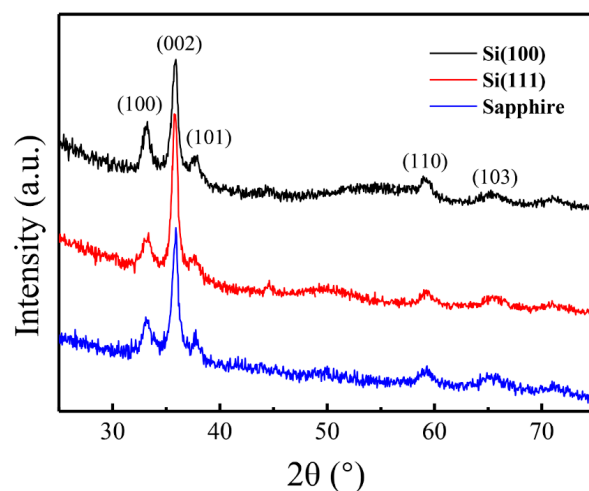


Figure 1. GIXRD patterns of AlN films grown on Si (100), Si (111), and sapphire substrates at 250°C .

Table 1. GIXRD results of AlN on different substrates, and the grain size of the samples by the Scherrer equation.

Substrates	2θ (°)	FWHM (°)	c (Å)	a (Å)	Grain Size (Å)
Si (100)	35.941	0.575	4.992	3.105	146.86
Si (111)	35.755	0.554	5.018	3.100	152.35
c-Al ₂ O ₃	35.899	0.530	4.999	3.122	159.31

The interplanar spacing, represented as “*d*”, which corresponds to the crystal planes associated with the 2θ angles observed in XRD patterns, can be calculated by utilizing Bragg’s equation for first-order diffraction [44]:

$$2d\sin\theta = n\lambda$$

where *d* can be expressed in terms of Miller indices (*h*, *k*, and *l*), “*λ*” denotes the X-ray wavelength (0.1540598 nm), and “*θ*” represents the angle of incidence.

The lattice constants “*a*” and “*c*” of hexagonal AlN can be determined using the following equation:

$$\frac{1}{d_{hkl}^2} = \frac{4}{3} \left(\frac{h^2 + hk + k^2}{a^2} \right) + \frac{l^2}{c^2}$$

Using the (002) orientation, the lattice constants “*c*” for AlN/Si (100), AlN/Si (111), and AlN /sapphire were determined as 4.992 Å, 5.018 Å, and 4.999 Å, respectively. These values are slightly larger than the bulk AlN value of 4.981 Å [44], but consistent with previous reports on AlN grown by ALD [45]. The difference between the *c*-axis values of the as-grown AlN may be attributed to the mismatch in their crystal structures and thermal properties [46]. Using the (100) orientation, the lattice constants “*a*” for AlN/Si (100), AlN/Si (111), and AlN /sapphire were calculated as 3.105 Å, 3.100 Å, and 3.122 Å, respectively, which is comparable to the bulk AlN value of 3.111 Å [44]. The formation of defects during thin film growth could be one of the main reasons for the lattice constant variations. These defects can include dislocations, dislocation pile-ups, grain boundaries, and interface defects between the film and the substrate. These defects can have an impact on the crystal lattice structure of the thin film, resulting in changes in the lattice constants.

The disparities of lattice constants are related to film strain. In this case, the strains parallel to the *c*-axis [$\epsilon^\perp = (c_{\text{epi}} - c_0)/c_0$] [47], for AlN grown on Si (100), Si (111), and sapphire, were determined to be 0.0022 GPa, 0.0074 Gpa, and 0.0036 GPa, respectively. This positive value indicates the presence of compressive strain, which means that the interplanar spacing along the *c*-axis is longer than that of unstrained AlN. The strains in the plane [$\epsilon^{\parallel} = (a_{\text{epi}} - a_0)/a_0$] were calculated as −0.0020 Gpa, −0.0030 Gpa and 0.0030 GPa, respectively. These negative values of ϵ^{\parallel} for AlN on Si suggest compressive strain in the in-plane directions, while the positive value for AlN on sapphire indicates tensile strain. This is because of the lattice mismatch of AlN between its substrates.

The average grain size of the sample was determined using the Scherrer equation [48], which relates the grain size (*D*) to the width of the peak at half of its maximum intensity (FWHM).

$$D = \frac{k\lambda}{B \cos\theta}$$

where *D* represents the average grain size (Å); *k* is the Scherrer constant, which is typically assumed to be 0.91, but may vary depending on the morphology of the crystal domains; *λ* is the X-ray wavelength, which depends on the type of X-ray used. In this study, the *λ* is 1.54058 Å (Cu Kα). *B* corresponds to the FWHM of the diffraction peak (radians), and *θ* represents the Bragg angle (radians). The average crystallite sizes for the (002) reflections of the AlN on Si (100), Si (111), and sapphire were calculated to be 146.86, 152.35, and 159.31 Å, respectively. The largest grain size of AlN/sapphire is indicated by the lowest FWHM of

the (002) peak. Moreover, the average grain size of AlN/Si (111) was slightly larger than that of AlN/Si (100). Larger grain size usually relates to improved crystallinity [43].

The XRR results depicted in Figure 2 exhibit clear Kiessig fringes for all the AlN samples, suggesting the sharp interfaces between the AlN films and substrates. By fitting the oscillation period and amplitude, the film's thickness and density can be calculated. The experimental data were analyzed using Globfit software with two-layer models, i.e., AlN/Si and AlN/sapphire. The XRR data presented in Figure 2a exhibit excellent agreement between the measured and simulated results for the AlN/Si (111) sample. The measured film thicknesses were 84 nm, 72 nm, and 68 nm for AlN on Si (100), Si (111), and sapphire substrates, respectively. The variation in film thicknesses for AlN deposited on different substrates suggests different growth rates on each substrate. The initial growth of ALD is strongly influenced by the outermost surface of the substrate, as it determines the nucleation and initial bonding during the growth process [19]. The first step of plasma treatment, in the experiment, refers to the process of introducing nitrogen atoms into the surface of a material. In the case of sapphire and Si surfaces, it is generally easier to nitride the Si surface compared to the sapphire surface. The main reason for this difference is the chemical nature of the two materials [49]. Si has a higher affinity for nitrogen compared to sapphire, resulting in more adsorption sites (or reactive groups) on the Si surface, which facilitates the subsequent AlN deposition. The critical angle (θ_c), a material-specific property mainly dependent on film density, is located at the first minima of the second derivative of the XRR intensity [50]. In Figure 2b–d, the θ_c of the as-grown AlN thin films are presented in the insets. The extracted critical angles for AlN on Si (100) and Si (111) substrates were 0.230° and 0.238° , respectively, while for AlN on sapphire, it was 0.242° ; these are a little higher than the reported values [51]. These critical angle values align with prior research on this topic. In addition, density values calculated from the simulations revealed that AlN/sapphire exhibits a density of 3.01 g/cm^3 , which is lower than the bulk material's mass density of 3.25 g/cm^3 , whereas those on Si (100) and Si (111) have densities of 2.81 and 2.86 g/cm^3 , respectively. These results match well with the values previously reported for AlN films produced using various deposition techniques, such as PEALD and magnetron sputtering [52,53]. The result also suggests that the substrate can influence the density of the deposited AlN film. The higher density of AlN on sapphire compared to that on Si can be attributed to the lattice mismatch and interfacial interactions between N plasma and the respective substrates. Sapphire has a closer lattice matching with AlN compared to Si, allowing for better deposition and stronger interfacial bonding. This leads to a more compact and dense structure in the AlN film on sapphire. The higher density of AlN on Si (111) compared to Si (100) can be attributed to the better matching of hexagonal AlN with the Si (111) plane, which possesses six-fold symmetry, compared to the Si (100) plane with four-fold symmetry.

The cross-sectional SEM micrograph of AlN/Si (100) is shown in Figure 3, revealing an AlN film thickness of around 85 nm. This value is consistent with the one obtained from XRR measurements. In addition, the AlN on Si (100) exhibits a uniform morphology and a flat interface. The surface features of the AlN were investigated by AFM, and the images are presented in Figure 4. The roughness of film surface is commonly assessed using the root-mean-square (RMS) value of the surface roughness [54]. The RMS surface roughness values for AlN deposited on Si (111), Si (100), and sapphire substrates were determined to be 0.95, 1.02, and 1.36 nm, respectively. The obtained results are below the values previously reported for ALD-grown AlN [41]. By comparing the RMS surface roughness values and average crystallite sizes (Table 1) for the different substrates, we can observe that the AlN film on sapphire substrate has the highest RMS surface roughness value (1.36 nm), and also has the highest average grain size (159.31 \AA). In contrast, AlN films on Si (111) substrates have the smallest RMS surface roughness value (0.95 nm) and the smallest average grain size (152.35 \AA). This implies that there is a positive correlation between RMS surface roughness and average grain size, indicating that films with larger grain size usually yield higher surface roughness. The effect of substrate on surface roughness and

grain growth is mainly due to the difference of lattice mismatch between AlN and substrate. The lattice mismatch between AlN and substrates is summarized in Table 2. In this case, AlN films on sapphire substrate show the largest RMS surface roughness and average grain size, possibly due to the better lattice match between substrate and AlN, which favors the growth of larger grains. However, AlN films on Si (111) and Si (100) substrates show lower surface roughness and smaller average grain size, which may be due to poor lattice matching.

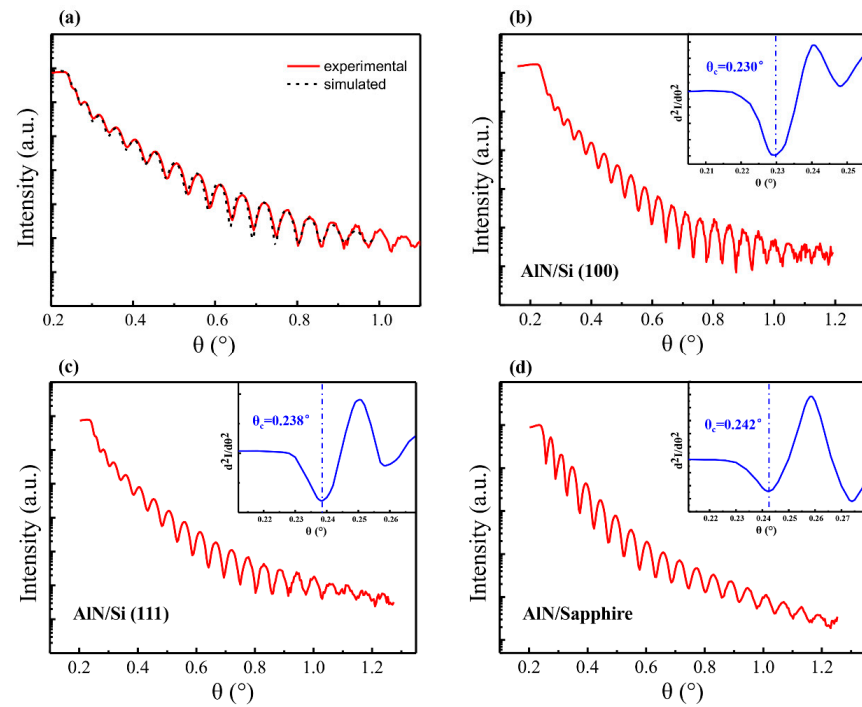


Figure 2. (a) Kiessig fringes of AlN on Si (111): solid and dotted lines illustrate experimental and fitted data, respectively. (b–d) X-ray reflectometry spectra for AlN thin films grown on Si (100), Si (111), and sapphire substrates, respectively.

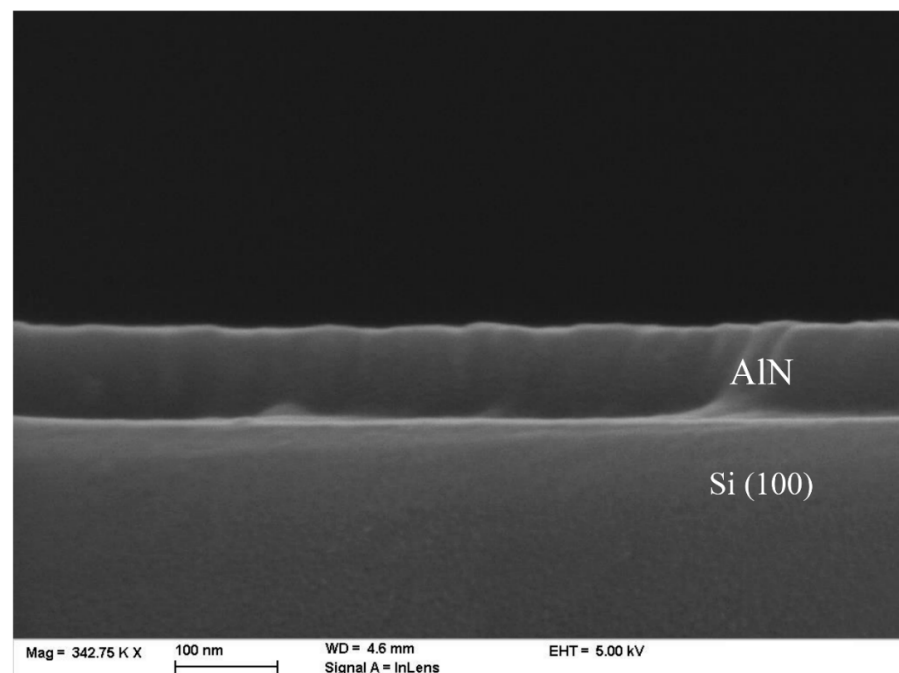


Figure 3. Cross-sectional SEM micrograph of the AlN film grown on Si (100).

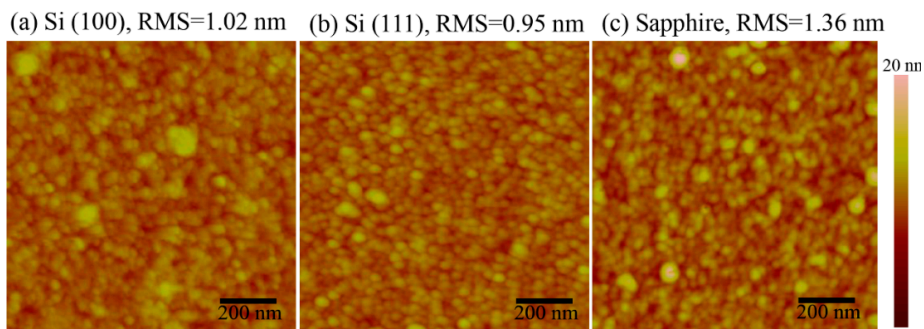


Figure 4. AFM image of AlN thin films grown on Si (100), Si (111), and sapphire substrates, respectively.

Table 2. The lattice parameters and lattice mismatch of AlN film and the substrates.

Materials	AlN	Sapphire	Si
Lattice constant (Å)	$a = 3.111$ $b = 4.981$	$a = 4.758$ $b = 12.99$	$a = 5.431$
Lattice Mismatch (with AlN)	—	+13.2%	−19.0%

Figure 5 presents a depth profile analysis of the AlN/Si (100). The results demonstrate that the atomic percentages of Al and N remain relatively constant throughout the film thickness in the etching direction. The Al and N contents in most AlN films are 47.2% and 52.0%, respectively, indicating that the membrane components are basically at the stoichiometric ratio. AlN contains a slightly higher proportion of nitrogen compared to aluminum. The higher nitrogen content in AlN is a result of the initial nitridation process, which involves the plasma-assisted breakdown of nitrogen gas [55]. The deposition process at a low temperature does not lead to the significant integration of carbon-containing ligands from the precursors, as indicated by the very low amount of carbon (0.7%) in the film. The content of oxygen in AlN is 1.1%, which is lower than the reported results [56], indicating negligible oxygen contamination. The main source of the high oxygen and carbon detected on the surface is atmospheric contamination.

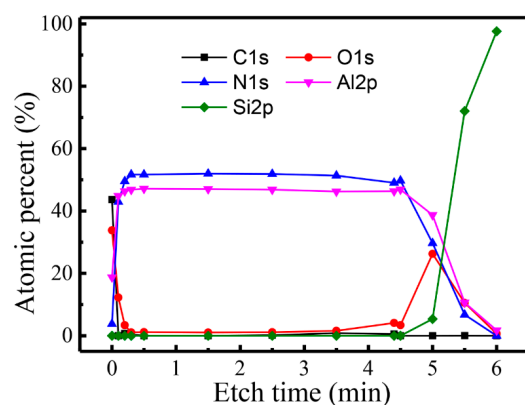


Figure 5. XPS depth profile of AlN thin films grown on Si (100).

The optical constants of AlN, such as refractive index (n) and extinction coefficient (k), were analyzed using SE. Figure 6 shows the dependence of n and k on the wavelength, ranging from 275 to 826 nm. The measurements reveal that at a wavelength of 532 nm, the n values of AlN films on Si (100), Si (111), and sapphire substrates are 1.967, 1.958, and 1.941, respectively. These values are below the bulk value ($n = 2.1$ at 533 nm) for single-crystal quality, but are consistent with the reported values of ALD-grown AlN [52]. In this case, AlN on Si has a higher n than that grown on sapphire. The wavelength of

$k = 0$, for AlN grown on both Si (100) and Si (111), is at 300 nm, with a rapid decrease between 275 and 300 nm. The zero of k value observed at higher wavelengths indicates that AlN/Si films remain transparent throughout the 300–826 nm range. Similarly, for AlN/sapphire, k decreases rapidly from 275 nm to 425 nm and becomes zero at 425 nm. Beyond this wavelength, k also remains at zero, indicating that AlN/sapphire films are transparent beyond a wavelength of 425 nm. These results suggest that AlN films grown on Si have a broader range of transparency wavelength than on sapphire substrates. The low absorption and high transparency are important factors for applications that require transparent materials in the ultraviolet range, such as photovoltaics, LEDs, and optical sensors. The transparency of the AlN films beyond these wavelengths also indicates that they may have potential for use as protective coatings or in optical devices that require high optical transparency in the visible range.

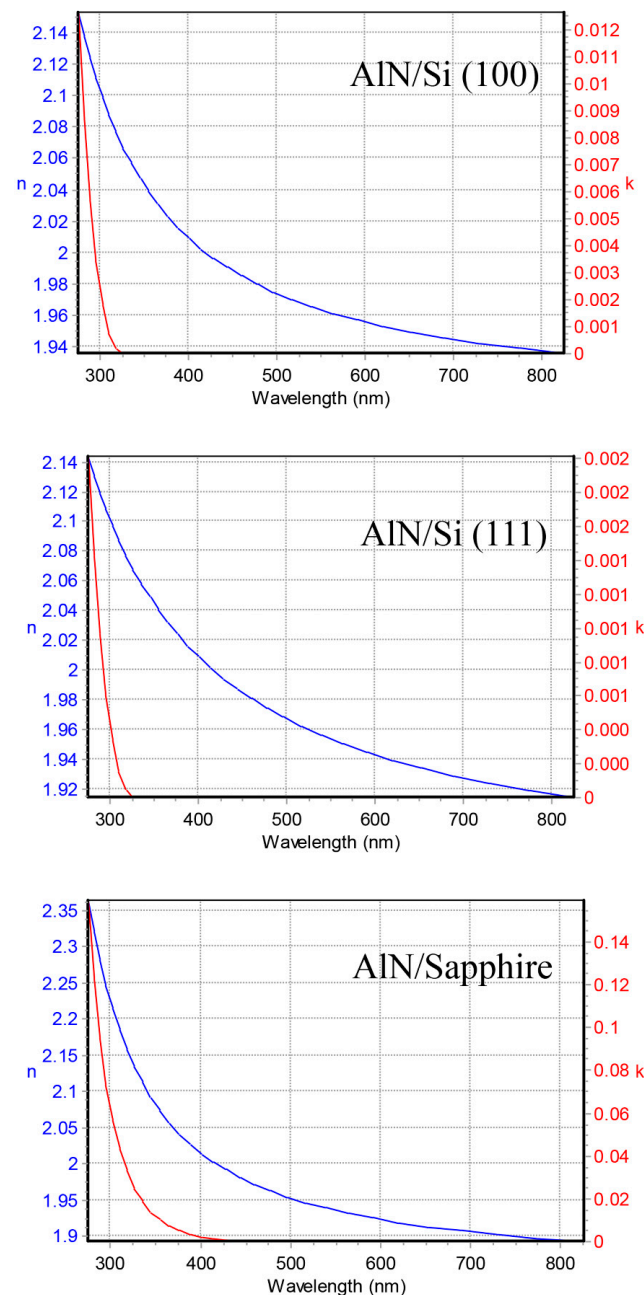


Figure 6. Refractive index and extinction coefficient of AlN films grown on different substrates as a function of wavelength.

4. Conclusions

In conclusion, the properties of PEALD-AlN deposited on Si (100), Si (111), and c-plane sapphire substrates were comparatively investigated. The results reveal that the as-grown AlN thin films possess a hexagonal wurtzite structure and are characterized as polycrystalline, regardless of the substrate. There is a certain relationship between the RMS surface roughness value and the average grain size, in which a larger RMS value is usually associated with a larger average grain size. The study also reveals that AlN/Si (100) has the highest n value at 532 nm, while AlN/sapphire exhibits a lower n value. Importantly, AlN films on both Si and sapphire substrates have a k value of zero within the visible range, indicating an optical transparency in the visible range. These results suggest that AlN thin films have significant potential for optoelectronic applications where optical transparency is a critical factor. This work of obtaining AlN films with smooth surfaces and sharp AlN/substrate interfaces is essential for their use as buffer layers in heteroepitaxy GaN.

Author Contributions: S.L. conceived and executed the project. Y.L. contributed XRR measurements and reviewed the manuscript. X.Z., J.T. and R.T. provided funding support for the project. S.L. performed the thin film deposition and XRD, SEM, and SE measurements; analyzed the data; and wrote the manuscript. All authors have read and agreed to the published version of the manuscript.

Funding: This work was supported by the Hunan Provincial Natural Science Foundation of China (Grant No. 2022JJ40163, Grant No. 2021JJ30298, Grant No. 2023JJ50283), the Education Department of Hunan Province (Grant No. 21B0598, Grant No. 22B0020), the Natural Science Foundation of China (Grant No. 52002021), Fundamental Research Funds for the Central Universities (Grant No. FRF-TP-20-016A2, Grant No. FRF-BR-20-02A), and Natural Science Foundation of Changsha (Grant No. kq2208213).

Data Availability Statement: The data that support the findings of this study are available from the corresponding author upon reasonable request.

Acknowledgments: We thank Gang Zhao from the School of Physics and Electronics, Hunan Normal University, for the XPS measurements.

Conflicts of Interest: The authors declare no conflict of interest.

References

1. Taniyasu, Y.; Kasu, M.; Makimoto, T. An aluminium nitride light-emitting diode with a wavelength of 210 nanometres. *Nature* **2006**, *441*, 325–328. [[CrossRef](#)]
2. Lu, J.; Chen, J.-T.; Dahlqvist, M.; Kabouche, R.; Medjdoub, F.; Rosen, J.; Kordina, O.; Hultman, L. Transmorphic epitaxial growth of AlN nucleation layers on SiC substrates for high-breakdown thin GaN transistors. *Appl. Phys. Lett.* **2019**, *115*, 221601. [[CrossRef](#)]
3. Zhang, D.; Cheng, X.; Shen, L.; Zheng, L.; Gu, Z.; Zhou, W.; Liu, X.; Yu, Y. Influence of Poly-AlN Passivation on the Performance Improvement of 3-MeV Proton-Irradiated AlGaIn/GaN MIS-HEMTs. *IEEE Trans. Nucl. Sci.* **2019**, *66*, 2215–2219. [[CrossRef](#)]
4. Ambacher, O. Growth and applications of Group III-nitrides. *J. Phys. D Appl. Phys.* **1998**, *31*, 2653. [[CrossRef](#)]
5. Amano, H.; Sawaki, N.; Akasaki, I.; Toyoda, Y. Metalorganic vapor phase epitaxial growth of a high quality GaN film using an AlN buffer layer. *Appl. Phys. Lett.* **1986**, *48*, 353–355. [[CrossRef](#)]
6. Liu, S.; Yang, S.; Tang, Z.; Jiang, Q.; Liu, C.; Wang, M.; Shen, B.; Chen, K.J. Interface/border trap characterization of Al₂O₃/AlN/GaN metal-oxide-semiconductor structures with an AlN interfacial layer. *Appl. Phys. Lett.* **2015**, *106*, 051605. [[CrossRef](#)]
7. Pan, L.; Dong, X.; Li, Z.; Luo, W.; Ni, J. Influence of the AlN nucleation layer on the properties of AlGaIn/GaN heterostructure on Si (1 1 1) substrates. *Appl. Surf. Sci.* **2018**, *447*, 512–517. [[CrossRef](#)]
8. Liudi Mulyo, A.; Rajpalke, M.K.; Vullum, P.E.; Weman, H.; Kishino, K.; Fimland, B.-O. The influence of AlN buffer layer on the growth of self-assembled GaN nanocolumns on graphene. *Sci. Rep.* **2020**, *10*, 853. [[CrossRef](#)]
9. Zhan, X.; Liu, J.; Sun, X.; Huang, Y.; Gao, H.; Zhou, Y.; Li, Q.; Sun, Q.; Yang, H. Crack-free 2.2 μm -thick GaN grown on Si with a single-layer AlN buffer for RF device applications. *J. Phys. D Appl. Phys.* **2023**, *56*, 015104. [[CrossRef](#)]
10. Yeadon, M.; Marshall, M.T.; Hamdani, F.; Pekin, S.; Morkoç, H.; Gibson, J.M. In situ transmission electron microscopy of AlN growth by nitridation of (0001) α -Al₂O₃. *J. Appl. Phys.* **1998**, *83*, 2847–2850. [[CrossRef](#)]
11. Zscherp, M.F.; Mengel, N.; Hofmann, D.M.; Lider, V.; Ojaghi Dogahe, B.; Becker, C.; Beyer, A.; Volz, K.; Schörmann, J.; Chatterjee, S. AlN Buffer Enhances the Layer Quality of MBE-Grown Cubic GaN on 3C-SiC. *Cryst. Growth Des.* **2022**, *22*, 6786–6791. [[CrossRef](#)]

12. Lutsenko, E.V.; Rzheutski, M.V.; Vainilovich, A.G.; Svitsiankou, I.E.; Shulenkova, V.A.; Muravitskaya, E.V.; Alexeev, A.N.; Petrov, S.I.; Yablonskii, G.P. MBE AlGaN/GaN HEMT Heterostructures with Optimized AlN Buffer on Al₂O₃. *Semiconductors* **2018**, *52*, 2107–2110. [[CrossRef](#)]
13. Zamir, S.; Meyler, B.; Zolotoyabko, E.; Salzman, J. The effect of AlN buffer layer on GaN grown on (111)-oriented Si substrates by MOCVD. *J. Cryst. Growth* **2000**, *218*, 181–190. [[CrossRef](#)]
14. Yarar, E.; Hrkac, V.; Zamponi, C.; Piorra, A.; Kienle, L.; Quandt, E. Low temperature aluminum nitride thin films for sensory applications. *AIP Adv.* **2016**, *6*, 075115. [[CrossRef](#)]
15. George, S.M. Atomic Layer Deposition: An Overview. *Chem. Rev.* **2010**, *110*, 111–131. [[CrossRef](#)] [[PubMed](#)]
16. Cremers, V.; Puurunen, R.L.; Dendooven, J. Conformality in atomic layer deposition: Current status overview of analysis and modelling. *Appl. Phys. Rev.* **2019**, *6*, 021302. [[CrossRef](#)]
17. Vervuurt, R.H.J.; Karasulu, B.; Verheijen, M.A.; Kessels, W.M.M.; Bol, A.A. Uniform Atomic Layer Deposition of Al₂O₃ on Graphene by Reversible Hydrogen Plasma Functionalization. *Chem. Mater.* **2017**, *29*, 2090–2100. [[CrossRef](#)]
18. Puurunen, R.L. Correlation between the growth-per-cycle and the surface hydroxyl group concentration in the atomic layer deposition of aluminum oxide from trimethylaluminum and water. *Appl. Surf. Sci.* **2005**, *245*, 6–10. [[CrossRef](#)]
19. Miikkulainen, V.; Leskelä, M.; Ritala, M.; Puurunen, R. ChemInform Abstract: Crystallinity of Inorganic Films Grown by Atomic Layer Deposition: Overview and General Trends. *J. Appl. Phys.* **2013**, *113*, 2. [[CrossRef](#)]
20. Profijt, H.B.; Potts, S.E.; van de Sanden, M.C.M.; Kessels, W.M.M. Plasma-Assisted Atomic Layer Deposition: Basics, Opportunities, and Challenges. *J. Vac. Sci. Technol. A* **2011**, *29*, 050801. [[CrossRef](#)]
21. Gakis, G.P.; Vahlas, C.; Vergnes, H.; Dourdain, S.; Tison, Y.; Martinez, H.; Bour, J.; Ruch, D.; Boudouvis, A.G.; Caussat, B.; et al. Investigation of the initial deposition steps and the interfacial layer of Atomic Layer Deposited (ALD) Al₂O₃ on Si. *Appl. Surf. Sci.* **2019**, *492*, 245–254. [[CrossRef](#)]
22. Lu, J.; Elam, J.W.; Stair, P.C. Atomic layer deposition—Sequential self-limiting surface reactions for advanced catalyst “bottom-up” synthesis. *Surf. Sci. Rep.* **2016**, *71*, 410–472. [[CrossRef](#)]
23. Zaera, F. Mechanisms of surface reactions in thin solid film chemical deposition processes. *Coord. Chem. Rev.* **2013**, *257*, 3177–3191. [[CrossRef](#)]
24. Lee, Y.J.; Kang, S.-W. Growth of aluminum nitride thin films prepared by plasma-enhanced atomic layer deposition. *Thin Solid Film.* **2004**, *446*, 227–231. [[CrossRef](#)]
25. Ozgit, C.; Donmez, I.; Alevli, M.; Biyikli, N. Self-limiting low-temperature growth of crystalline AlN thin films by plasma-enhanced atomic layer deposition. *Thin Solid Film.* **2012**, *520*, 2750–2755. [[CrossRef](#)]
26. Van Bui, H.; Wiggers, F.B.; Gupta, A.; Nguyen, M.D.; Aarnink, A.A.I.; de Jong, M.P.; Kovalgin, A.Y. Initial growth, refractive index, and crystallinity of thermal and plasma-enhanced atomic layer deposition AlN films. *J. Vac. Sci. Technol. A* **2014**, *33*, 01A111. [[CrossRef](#)]
27. Banerjee, S.; Aarnink, A.A.I.; van de Kruijs, R.; Kovalgin, A.Y.; Schmitz, J. PEALD AlN: Controlling growth and film crystallinity. *Phys. Status Solidi C* **2015**, *12*, 1036–1042. [[CrossRef](#)]
28. Bosund, M.; Sajavaara, T.; Laitinen, M.; Huhtio, T.; Putkonen, M.; Airaksinen, V.-M.; Lipsanen, H. Properties of AlN grown by plasma enhanced atomic layer deposition. *Appl. Surf. Sci.* **2011**, *257*, 7827–7830. [[CrossRef](#)]
29. Kim, Y.; Kim, M.S.; Yun, H.J.; Ryu, S.Y.; Choi, B.J. Effect of growth temperature on AlN thin films fabricated by atomic layer deposition. *Ceram. Int.* **2018**, *44*, 17447–17452. [[CrossRef](#)]
30. Nguyen, T.; Adjeroud, N.; Glinsek, S.; Fleming, Y.; Guillot, J.; Grysan, P.; Polesel-Maris, J. A film-texture driven piezoelectricity of AlN thin films grown at low temperatures by plasma-enhanced atomic layer deposition. *APL Mater.* **2020**, *8*, 071101. [[CrossRef](#)]
31. Liu, X.; Ramanathan, S.; Lee, E.; Seidel, T.E. Atomic Layer Deposition of Aluminum Nitride Thin films from Trimethyl Aluminum (TMA) and Ammonia. *MRS Online Proc. Libr.* **2003**, *811*, 158–163.
32. Tarala, V.; Altakhov, A.; Martens, V.; Lisitsyn, S. Growing aluminum nitride films by Plasma-Enhanced Atomic Layer Deposition at low temperatures. *J. Phys. Conf. Ser.* **2015**, *652*, 012034. [[CrossRef](#)]
33. Shih, H.-Y.; Lee, W.-H.; Kao, W.-C.; Chuang, Y.-C.; Lin, R.-M.; Lin, H.-C.; Shiojiri, M.; Chen, M.-J. Low-temperature atomic layer epitaxy of AlN ultrathin films by layer-by-layer, in-situ atomic layer annealing. *Sci. Rep.* **2017**, *7*, 39717. [[CrossRef](#)]
34. Legallais, M.; Mehdi, H.; David, S.; Bassani, F.; Labau, S.; Pelissier, B.; Baron, T.; Martinez, E.; Ghibaudo, G.; Salem, B. Improvement of AlN Film Quality Using Plasma Enhanced Atomic Layer Deposition with Substrate Biasing. *ACS Appl. Mater. Interfaces* **2020**, *12*, 39870–39880. [[CrossRef](#)]
35. Kim, H.; Kim, N.D.; An, S.C.; Yoon, H.J.; Choi, B.J. Improved interfacial properties of thermal atomic layer deposited AlN on GaN. *Vacuum* **2019**, *159*, 379–381. [[CrossRef](#)]
36. Kim, H.; Yun, H.J.; Choi, S.; Choi, B.J. Comparison of electrical and interfacial characteristics between atomic-layer-deposited AlN and AlGaIn on a GaN substrate. *Appl. Phys. A* **2020**, *126*, 449. [[CrossRef](#)]
37. Van Bui, H.; Nguyen, M.D.; Wiggers, F.B.; Aarnink, A.A.I.; de Jong, M.P.; Kovalgin, A.Y. Self-Limiting Growth and Thickness- and Temperature- Dependence of Optical Constants of ALD AlN Thin Films. *ECS J. Solid State Sci. Technol.* **2014**, *3*, P101. [[CrossRef](#)]
38. Schilirò, E.; Giannazzo, F.; Bongiorno, C.; Di Franco, S.; Greco, G.; Roccaforte, F.; Prystawko, P.; Kruszewski, P.; Leszczyński, M.; Krysko, M.; et al. Structural and electrical properties of AlN thin films on GaN substrates grown by plasma enhanced-Atomic Layer Deposition. *Mater. Sci. Semicond. Process.* **2019**, *97*, 35–39. [[CrossRef](#)]

39. Liu, S.; Peng, M.; Hou, C.; He, Y.; Li, M.; Zheng, X. PEALD-Grown Crystalline AlN Films on Si (100) with Sharp Interface and Good Uniformity. *Nanoscale Res. Lett.* **2017**, *12*, 279. [[CrossRef](#)]
40. Lei, W.; Chen, Q. Crystal AlN deposited at low temperature by magnetic field enhanced plasma assisted atomic layer deposition. *J. Vac. Sci. Technol. A* **2012**, *31*, 01A114. [[CrossRef](#)]
41. Alevli, M.; Ozgit, C.; Donmez, I.; Biyikli, N. The influence of N₂/H₂ and ammonia N source materials on optical and structural properties of AlN films grown by plasma enhanced atomic layer deposition. *J. Cryst. Growth* **2011**, *335*, 51–57. [[CrossRef](#)]
42. Iriarte, G.F.; Reyes, D.F.; González, D.; Rodríguez, J.G.; García, R.; Calle, F. Influence of substrate crystallography on the room temperature synthesis of AlN thin films by reactive sputtering. *Appl. Surf. Sci.* **2011**, *257*, 9306–9313. [[CrossRef](#)]
43. García-Méndez, M.; Morales-Rodríguez, S.; Shaji, S.; Krishnan, B.; Bartolo-Pérez, P. Structural properties of AlN films with oxygen content deposited by reactive magnetron sputtering: XRD and XPS characterization. *Surf. Rev. Lett.* **2011**, *18*, 23–31. [[CrossRef](#)]
44. Moram, M.A.; Vickers, M.E. X-ray diffraction of III-nitrides. *Rep. Prog. Phys.* **2009**, *72*, 036502. [[CrossRef](#)]
45. Österlund, E.; Seppänen, H.; Bepalova, K.; Miikkulainen, V.; Paulasto-Kröckel, M. Atomic layer deposition of AlN using atomic layer annealing—Towards high-quality AlN on vertical sidewalls. *J. Vac. Sci. Technol. A* **2021**, *39*, 032403. [[CrossRef](#)]
46. Sun, C.J.; Kung, P.; Saxler, A.; Ohsato, H.; Haritos, K.; Razeghi, M. A crystallographic model of (00·1) aluminum nitride epitaxial thin film growth on (00·1) sapphire substrate. *J. Appl. Phys.* **1994**, *75*, 3964–3967. [[CrossRef](#)]
47. Zhou, S.Q.; Vantomme, A.; Zhang, B.S.; Yang, H.; Wu, M.F. Comparison of the properties of GaN grown on complex Si-based structures. *Appl. Phys. Lett.* **2005**, *86*, 081912. [[CrossRef](#)]
48. Scherrer, P. Bestimmung der Größe und der inneren Struktur von Kolloidteilchen mittels Röntgenstrahlen. *Nachr. Von Der Ges. Der Wiss. Zu Göttingen Math. Phys. Kl.* **1918**, *1918*, 98–100.
49. Dovidenko, K.; Oktyabrsky, S.; Narayan, J.; Razeghi, M. Aluminum nitride films on different orientations of sapphire and silicon. *J. Appl. Phys.* **1996**, *79*, 2439–2445. [[CrossRef](#)]
50. Chason, E.; Mayer, T.M. Thin film and surface characterization by specular X-ray reflectivity. *Crit. Rev. Solid State Mater. Sci.* **1997**, *22*, 1–67. [[CrossRef](#)]
51. Motamedi, P.; Cadien, K. Structural and optical characterization of low-temperature ALD crystalline AlN. *J. Cryst. Growth* **2015**, *421*, 45–52. [[CrossRef](#)]
52. Alevli, M.; Ozgit, C.; Donmez, I.; Biyikli, N. Structural properties of AlN films deposited by plasma-enhanced atomic layer deposition at different growth temperatures. *Phys. Status Solidi A* **2012**, *209*, 266–271. [[CrossRef](#)]
53. Venkataraj, S.; Severin, D.; Drese, R.; Koerfer, F.; Wuttig, M. Structural, optical and mechanical properties of aluminium nitride films prepared by reactive DC magnetron sputtering. *Thin Solid Film.* **2006**, *502*, 235–239. [[CrossRef](#)]
54. Martin, Y.; Williams, C.C.; Wickramasinghe, H.K. Atomic force microscope—force mapping and profiling on a sub 100-Å scale. *J. Appl. Phys.* **1987**, *61*, 4723–4729. [[CrossRef](#)]
55. Liu, S.; Zhao, G.; He, Y.; Wei, H.; Li, Y.; Qiu, P.; Song, Y.; An, Y.; Wang, X.; Wang, X.; et al. Interfacial Tailoring for the Suppression of Impurities in GaN by In Situ Plasma Pretreatment via Atomic Layer Deposition. *ACS Appl. Mater. Interfaces* **2019**, *11*, 35382–35388. [[CrossRef](#)]
56. Motamedi, P.; Cadien, K. XPS analysis of AlN thin films deposited by plasma enhanced atomic layer deposition. *Appl. Surf. Sci.* **2014**, *315*, 104–109. [[CrossRef](#)]

Disclaimer/Publisher’s Note: The statements, opinions and data contained in all publications are solely those of the individual author(s) and contributor(s) and not of MDPI and/or the editor(s). MDPI and/or the editor(s) disclaim responsibility for any injury to people or property resulting from any ideas, methods, instructions or products referred to in the content.